Step-step interactions on GaAs (110) nanopatterns

B. Galiana, M. Benedicto, and P. Tejedor[a)]
Instituto de Ciencia de Materiales de Madrid, C.S.I.C., Sor Juana Inés de la Cruz 3, 28049 Madrid, Spain

(Received 13 July 2012; accepted 17 December 2012; published online 9 January 2013)

The step-step interactions on vicinal GaAs (110) surface patterns have been extracted from the quantitative analysis of the terrace width distribution (TWD). We have specifically studied the interactions in near-equilibrium faceting and kinetics-driven step bunching and meandering formed by spontaneous self-organization or through the modification of GaAs growth kinetics by atomic hydrogen. We show that the experimental TWDs determined from atomic force microscopy measurements can be accurately described by a weighed sum of a generalized Wigner distribution and several Gaussians. The results of our calculations indicate that straight facets are formed during high temperature homoepitaxy due to attractive interactions between $[1\bar{1}0]$ steps. At low temperatures, steady state attractive interactions in $[1\bar{1}0]$ step bunches are preceded by a transition regime dominated by entropic and energetic repulsions between meandering $[1\bar{1}n]$-type steps ($n \geq 2$), whose population density exceeds that of the $[1\bar{1}0]$ bunched steps. In addition, it has been found that atomic H reduces the attractive interactions between $[1\bar{1}0]$ bunched steps and enhances entropic and dipole-induced energetic repulsions between H-terminated $[1\bar{1}n]$ steps through the inhibition of As–As bond formation at step edges. Our analysis has evidenced a correlation between the value of the adjustable parameter that accounts in our model for the specific weight of the secondary peaks in the TWD (β) and the extent of transverse meandering on the vicinal surface. © *2013 American Institute of Physics*. [http://dx.doi.org/10.1063/1.4774215]

I. INTRODUCTION

Epitaxial growth by step propagation on a vicinal surface is often affected by morphological instabilities such as step meandering and step bunching, which find their practical application in the fabrication of nanopatterned substrates for selective nucleation of metallic or semiconducting nanostructures.[1–3] Such instabilities appear when the energy barriers associated with adatom attachment to steps differ for adatoms approaching a step from opposite directions, i.e., Ehrlich-Schwoebel (E-S) effect.[4,5] Preferential attachment of adatoms to upper step edges equalizes the surface terrace widths, but makes steps unstable towards transverse meandering because matter is more likely to attach to advanced parts of the step edge. Steps can meander collectively fluctuating in-phase from the outset of growth, as described by the Bales-Zangwill model,[6] or they can initially meander with random phase and exhibit an increasing phase correlation with time as result of the kink-Ehrlich-Schwoebel effect (KESE).[7] Preferential attachment of adatoms to descending step edges, on the other hand, causes the train of initially equidistant steps to separate into large terraces and regions of high density step bunches through a variety of atomic mechanisms that include, pinning of steps by impurities, diffusion anisotropy, dimmer mobility, or step edge diffusion, among others.[8,9]

The analysis of the terrace width distribution (TWD), which gives the probability of finding a terrace of width W on the surface, is one of the best methods for experimentally determining the step-step interactions during unstable homoepitaxial growth of surface nanopatterns. Experimental studies have demonstrated that the TWD can be artificially modified to fabricate surface patterns with improved lateral uniformity by exposing the surface to certain surfactant agents like atomic hydrogen that induce changes in adatom attachment kinetics during growth.[10] Theoretical attempts to determine the strength of step-step interactions from the TWD have produced different results depending on the specific approximation employed.[11–15] The distribution of interstep distances is the result of both step fluctuations and step-step energetic interactions. The latter can occur through various mechanisms of elastic, dipolar or indirect electronic nature and, therefore, they can be attractive or repulsive. Due to the non-crossing condition of steps, fluctuations induce a decrease in configurational entropy whenever two steps get closer to each other, leading to an effective entropic repulsion between them.

The general analytical procedure used to extract quantitative information from TWD data when very strong repulsive interactions of entropic and/or energetic nature exist between neighbouring steps is based on the mean-field-like Gruber-Mullins approximation.[11,12] If the step-step interactions are sufficiently strong, terrace width fluctuations will be negligible. The TWD in this case will only sample the parabolic part of the confining potential and, consequently, it will be accurately described by a Gaussian:

$$P(W) = \frac{1}{\sigma\sqrt{2\pi}} \exp\left[-\frac{((W/W_0)-1)^2}{2\sigma^2}\right]. \quad (1)$$

Here, W_0 is the average terrace width and σ^2 is the variance of the Gaussian distribution. But if moderate repulsive or

[a)]Author to whom correspondence should be addressed. Electronic mail: ptejedor@icmm.csic.es.

attractive interactions exist, the terrace width distribution skews and the mean-field approximation cannot be used to accurately fit the experimental data. In this case, a more rigorous treatment of the step interactions is possible by means of the so-called Wigner surmise, a simple, single-parameter analytic expression rooted in random matrix theory,[16] which provides a superb approximation to the TWD for the three values of the step interaction strength, A_{Wigner}, for which the problem can be solved exactly, i.e., $-1/4$, 0, or 2.[17,18] Its explicit form is

$$P(W) = a_\rho \left(\frac{W}{W_0}\right)^\rho \exp\left[-b_\rho \left(\frac{W}{W_0}\right)^2\right], \tag{2}$$

where the constants a_ρ and b_ρ are defined in terms of Γ functions

$$\frac{a_\rho = 2b_\rho^{(\rho+1)/2}}{\Gamma((\rho+1)/2),} \tag{3}$$

$$b_\rho = \left[\frac{\Gamma((\rho+2)/2)}{\Gamma((\rho+1)/2)}\right]^2. \tag{4}$$

The single adjustable parameter ρ is related to the step-step interaction strength, A_{Wigner}, through the equation

$$A_{Wigner} = 1/4 \times (\rho - 2)\rho. \tag{5}$$

According to this equation, when $\rho > 2$, A_{Wigner} is positive and the effective step interactions are repulsive, while for $\rho < 2$, A_{Wigner} is negative and the interaction is attractive. In the particular case of $\rho = 2$ ($A_{Wigner} = 0$), the TWD describes a vicinal surface where only entropic interactions between steps exist.

The so-called generalized Wigner distribution (GWD),[13] defined by the simple assumption that Eqs. (2) and (5) are valid for all values of the interaction strength, allows to interpolate between the three special cases mentioned above.[19–21] However, this assumption is only reasonable when A_{Wigner} has positive or weakly negative values.[22] The generalized Wigner surmise has been applied in the past to extract quantitative information on the step-step interactions from the terrace width distribution on Cu (100), Cu (111), Pt (110), and Si (111) vicinal surfaces.[23–25]

This paper makes the first attempt to empirically quantify the step-step interaction strength in different self-organized nanopatterns formed by homoepitaxial growth on the GaAs (110) vicinal surface from the analysis of the terrace width distribution. In the following, we present our TWD fitting approximation, followed by a description of the molecular beam epitaxy experiments and the atomic force microscopy measurements of the terrace lengths. The results of three different sets of GaAs (110) nanopatterns grown under various kinetic regimes are then presented and discussed. Specifically, we analyze the interactions between steps that lead to the formation of step bunches, step meanders, and facets by spontaneous self-organisation or through the modification of adatom kinetics on the vicinal GaAs (110) surface by atomic hydrogen, used as a surfactant prior or during epitaxy. The final section offers a brief conclusion.

II. TWD FITTING APPROXIMATION

The fitting approximation used in the present work takes into account the coexistence of both step-step energetic interactions (attractive or repulsive) and entropic repulsions, i.e., step fluctuations. As it will be shown in Sec. IV, the TWD generally exhibits a main peak in the high step density region (low W values) and a number of secondary peaks or shoulders at larger W. The main peak, which is generally associated with weak step-step interactions,[19–21] has been fitted to a weighted sum of a Wigner and a Gaussian, as described in the theoretical work by Videcoq *et al.*[19] These authors used kinetic Monte Carlo (KMC) simulations to analyze the temporal evolution of the TWD during step bunching on a vicinal surface, taking into consideration just the entropic repulsion between steps. In the presence of step barriers, their model showed two distinct regimes. In one of them, additional repulsive step-step interactions associated with step meandering resulted from the asymmetry in adatom incorporation kinetics, leading to damped oscillations in the TWD. In the second regime growth induced effective attractive interactions between steps, leading to step bunching. Simulations of the TWD temporal evolution in the latter growth regime showed that the TWD was initially Gaussian and widened as step pairing took place. As the bunching instability developed, the TWD became first asymmetric towards the smaller terraces and then bimodal. At this point, fitting of the TWD to a single Gaussian was no longer possible and a weighted sum of a generalized Wigner distribution and a Gaussian distribution was required to describe the step bunches and the large terraces between them, respectively.

The secondary peaks (1 or 2 damped oscillations) that appear in the low step density region (high W values) of the TWD whenever the step bunching instability coexists on the vicinal GaAs (110) surface with transverse meandering or faceting along crystallographic directions different from the main one, i.e., $[1\bar{1}0]$, have been fitted to a sum of Gaussian functions in this work. Experimental and theoretical studies relative to these peaks are scarce in the literature, since most TWDs published to date are monomodal. In those few cases where multimodal TWDs have been reported, the microscopic origin of the secondary peaks has been attributed to a variety of phenomena, including the onset of faceting,[26] step-step attractions,[27] step-step repulsions,[19] or long-range elastic repulsions.[28]

In the present work, the experimental TWD is fitted to the following general equation:

$$\begin{aligned} \mathrm{TWD} = \mathrm{P(W)} &= \gamma \times [\alpha \times \mathrm{G}_{\mathrm{W}_{\mathrm{Wigner}}}(\mathrm{W}) + (1-\alpha) \\ &\times \Phi_{\mathrm{W}_{\mathrm{G\_short}}}(\mathrm{W})] + \sum_{\mathrm{n}=1}^{\mathrm{N}} [\beta_{\mathrm{n}} \times \Phi_{\mathrm{W}^{\mathrm{n}}_{\mathrm{G\_large}}}(\mathrm{W})], \\ \text{where } \sum_{\mathrm{n}=1}^{\mathrm{N}} \beta_{\mathrm{n}} &= \beta \text{ and } \gamma + \beta = 1. \end{aligned} \tag{6}$$

In this equation, α, β, and γ are the parameters to be fitted. Parameter β represents the weight of the N secondary peaks in the large terrace width region fitted to Gaussian functions and γ gives the weight of the mean peak area, thus allowing the comparison between weak (γ) and strong (β) step-step interactions. The value of α in turn gives the relative weight of the GWD with respect to γ, as defined in Ref. 19. By fitting the TWD, and using the relationship between the parameter ρ in the GWD and the interaction strength given by Eq. (5), the effective step-step interaction for each particular growth scenario is determined.

III. EXPERIMENTAL

All GaAs samples studied here were grown from As_4 and Ga beams in a solid-source VARIAN-360 MBE system. Atomic hydrogen was generated in the growth chamber by dissociation of H_2 gas in a W filament cracker cell at 1800 °C. Epiready GaAs (110) substrates misoriented 2° towards (111) A were indium bonded to Mo disks and outgassed at 350 °C before the surface oxide was removed by thermal desorption at a substrate temperature of 620 °C or by reaction with atomic hydrogen at 450 °C, under an As_4 flux of 2.5×10^{15} molecules cm^{-2} s^{-1}. GaAs layers having thicknesses between 5 and 120 nm (25–600 ML in the (110) direction) where grown at 430 °C and 620 °C. The Ga flux was 8.75×10^{13} atoms cm^{-2} s^{-1} in all experiments, while the As_4 flux was varied to give V:III flux ratios of 30 and 10, respectively. The GaAs growth rate on the (110) surface was 0.2 ML s^{-1} under these conditions. Three sets of samples were grown, hereafter named as A, B, and C. Set A (film thickness: 300 ML) was grown at high temperature, 620 °C, with a V:III flux ratio of 10. Set B (film thicknesses: 100, 200, and 600 ML) was grown at low temperature, 430 °C, under As-rich conditions with a V:III flux ratio of 30 after thermal desorption of the native oxide. Finally, set C (film thicknesses: 25, 50, and 500 ML) was prepared under the same growth conditions as set B after atomic H-assisted cleaning of the native oxide.

The surface topography of the GaAs (110) layers was examined with a Nanotec Electrónica S.L. AFM microscope operating in tapping mode under ambient conditions. We used single-crystalline Si AFM probes (Nanosensors, PPP-NCHR) with a nominal spring constant of 42 N/m and typical resonance frequency of 330 kHz. The tip had a nominal end radius of 8 ± 2 nm and a sidewall angle of 22.5 ± 2 nm. Accordingly, the topography resolution was approximately 4 nm.[29] The imaging scan rate was $\leq$0.5 Hz for a $3\ \mu m \times 3\ \mu m$ scan area and was adjusted to an appropriate imaging frequency for smaller scan sizes. Data acquisition was carried out at 512 points per scan line.

Quantitative analysis of the AFM images was performed using the WSxM™ SPM software from Nanotech Electrónica S.L. Fig. 1 illustrates the method used to determine the terrace width value (W) from a cross-section scan, according to the schematic shown in Fig. 1(a), for two different scenarios; Fig. 1(b) corresponds to a sample with well-developed kinetic step bunches and wide terraces, while Fig. 1(c) corresponds to a near-equilibrium faceted surface with narrow terraces. Each experimental TWD presented in this work is the result of 200 cross-section profiles along the [001] tilt direction of the vicinal surface, randomly measured across $1 \times 1\ \mu m^2$ or $3 \times 3\ \mu m^2$ images. Analysis of $3 \times 3\ \mu m^2$ images was only necessary for series B, due to the large average terrace sizes found in these samples. The W data set thus obtained is then plotted as a histogram. For all images, the number of bins was kept constant (10) to have a comparable data density in each of them. Consequently, the bin size is given by the maximum terrace width value extracted from the cross-section scan analysis. Finally, the best fit of

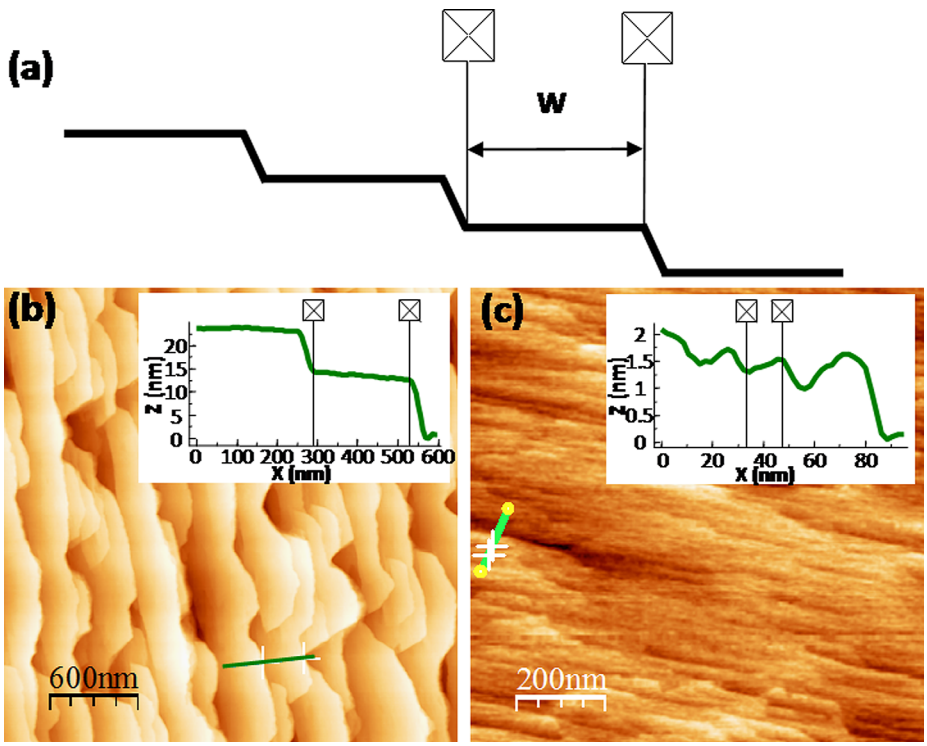

FIG. 1. Quantitative analysis of AFM images for terrace width determination. Schematic of terrace width measurement from a the cross-section scan profile (a) and application to different surface morphologies: low temperature kinetic step bunching and meandering exhibiting large terraces (b) and high-temperature faceted surface with narrow terraces (c).

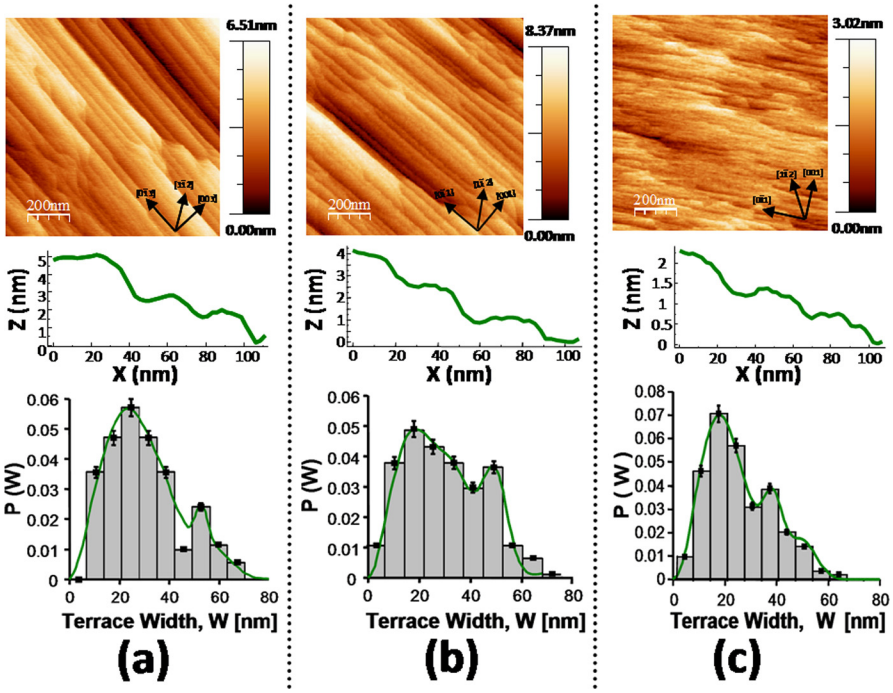

FIG. 2. AFM images (1 μm × 1 μm) of the GaAs (110) surface morphology, typical cross-section profiles along the [001] tilt direction with the resulting terrace width histograms and the corresponding TWD simulations (solid line) for the three samples in series A (300 ML GaAs deposition at 620 °C, As/Ga: 10): (a) conventional MBE growth, (b) H-assisted oxide desorption and conventional MBE growth, and (c) H-assisted oxide desorption and H-MBE growth.

the adjustable parameters α, β, and γ in Eq. (6) to the experimental TWDs obtained by the procedure described above allows the quantitative determination of the step-step interaction strength (A_{Wigner}) as well as its repulsive or attractive nature.

IV. RESULTS AND DISCUSSION

A series of 300 ML thick GaAs samples were grown at 620 °C with an As:Ga flux ratio of 10 (set A) to study the effect of atomic hydrogen irradiation on the TWD and the step-step interactions during faceting under near equilibrium conditions. A first sample was prepared by thermal desorption of the surface oxide and conventional MBE growth (sample I), a second sample was cleaned by H-assisted oxide etching followed by conventional MBE growth (sample II), and a third one was prepared by H-assisted oxide desorption and H-assisted MBE growth (sample III). In Fig. 2, we present a 1 μm × 1 μm AFM image of the surface morphology together with the experimental TWD histogram and the simulated TWD (solid line) corresponding to the fitting parameters gathered in Table I for all three samples. As shown in the images, all samples grown at high temperature exhibit terraces bounded by rather straight bunched steps along the $[1\bar{1}0]$ direction. Exposure to the atomic H beam, particularly when this is maintained during epitaxial growth, results in the reduction of the average terrace size, W_0, and hence the average height of the bunched step in the tilt direction, s_H (Table I). In addition, a tendency to form shorter terraces, laterally bounded by $[1\bar{1}2]$ steps edges, is found in those samples which had been exposed to H. The observed changes in terrace size are attributed to the shorter effective diffusion length of adatoms on the H-terminated surface that arises from the faster As incorporation kinetics to the surface through the formation of AsH_x intermediates.[30]

Upon fitting the experimental TWD data of the sample grown by conventional MBE (sample I) with the parameters α, β, and γ shown in Table I, we determined for the main peak centred at 27 nm a value of $\rho = 1.5$, which corresponds to an effective attractive interaction between steps of $A_{Wigner} = -0.19$. It is worth noting here the good agreement in TWD behaviour that exists between this sample and the simulations of high temperature step bunching (faceting) in the absence of step fluctuations described in Ref. 19, where a value of $\rho = 1.4$ was determined for a similar relative weight of the Wigner distribution ($\alpha = 98\%$).

Fitting of the main peak at 19 nm with the parameters shown in Table I for the GaAs (110) sample cleaned with atomic H (sample II) rendered a value of $\rho = 1.85$, corresponding to an attractive interaction between steps of

TABLE I. Fitting parameters used to simulate the experimental TWDs shown in Fig. 2 corresponding to **series A:** 300 ML GaAs (110) grown at 620 °C with an As/Ga flux ratio of 10 for three different experimental conditions: (I) conventional MBE growth, (II) H-assisted oxide desorption and conventional MBE growth, and (III) H-assisted oxide desorption and H-MBE growth.

	Main peak							Secondary peaks				
Sample	γ (%)	W_{Wigner} (nm)	ρ	A_{Wigner}	α (%)	W_{G_short} (nm)	σ	β (%)	W_{G_large} (nm)	σ	S_H (nm)	W_0 (nm)
I	99.0 ± 0.3	27 ± 3	1.5 ± 0.1	0.190 ± 0.001	94.0 ± 0.1	39 ± 2	2 ± 1	1.0 ± 0.3	53 ± 3	2.5 ± 0.3	1 ± 0.7	32.4 ± 0.1
II	73 ± 8	19 ± 3	1.85 ± 0.05	−0.07 ± 0.05	86 ± 1	32 ± 4	4 ± 2	27 ± 8	45 ± 4	4.5 ± 0.5	0.9 ± 0.5	31.6 ± 0.1
III	87 ± 5	18 ± 2	1.95 ± 0.01	−0.02 ± 0.01	82 ± 1	39 ± 4	4 ± 1	13 ± 5	50 ± 2	5.2 ± 0.5	0.4 ± 0.2	26.7 ± 0.2

$A_{Wigner} = -0.07$. In comparison, the value of the ρ parameter obtained from fitting the main peak at 18 nm for the sample exposed to H both during cleaning and epitaxy (sample III) is larger, i.e., $\rho = 1.95$, thus resulting in an attractive interaction strength of $A_{Wigner} = -0.02$. Therefore, GaAs growth on the vicinal surface exposed to atomic H leads to weaker attractive interactions between steps and this effect becomes more significant for high H coverages, i.e., longer exposure times to the atomic H beam.[31] Moreover, the marked tendency towards $\rho = 2$ with prolonged H exposure observed in samples II and III evidences the contribution of this adsorbate to create strong entropic repulsions between steps, consistent with the narrower terrace widths found in both samples.

In order to better understand the origin of the observed change in step-step interactions during growth on the H-terminated GaAs (110) vicinal surface, it is necessary to take into consideration the modifications introduced in the kinetics of adatom incorporation to steps by the surfactant action of atomic H reported in previous works.[10,30] Under the experimental conditions specified for sample I, conventional MBE proceeds by preferential incorporation of adatoms to the more reactive $[1\bar{1}0]$ surface steps, where stable (001) nanofacets with As-As dimers are formed by step bunching. The observed TWD thus describes mainly the effective attraction between $[1\bar{1}0]$ steps within the (001) nanofacets, since long-range repulsive interactions between bunches, accounted for by the secondary peak, are negligible in this sample. Exposure of the vicinal surface to the atomic H beam during cleaning of the surface oxide results in the chemisorption of H on the (110) terraces and the $[1\bar{1}0]$-step edges with Ga–H and As–H bond formation. As growth proceeds and step bunches develop, a fraction of the surface atoms remain bonded to H due to the surfactant action of the latter. This implies that the formation of As-As dimers on the (001) nanofacets is less favored and the attractive interactions between steps in the bunch are weakened, as we observe in sample II. When growth takes place under a continuous supply of H (sample III) the fraction of surface atoms bonded to H is much higher and, consequently, the probability of As–As bond formation is reduced. As a result, the effective step-step attractions in the bunch are much weaker, in accordance with the tendency towards debunching of $[1\bar{1}0]$ steps evidenced by the AFM scan profile in Fig. 2(c). In addition, energetic (dipole-induced) interactions between adjacent H-terminated $[1\bar{1}0]$ steps are likely to become more relevant as the H coverage increases, originating repulsions within the bunches, in good agreement with the ρ values derived from the TWD fit.

In turn, long-range repulsive interactions between bunched steps can be analysed by quantifying the relative weight of the secondary peaks (β) located in the low step density region of the TWD.[22,28] As we show in Table I, the value of β for the sample grown by conventional MBE is very low (1%), implying that in this particular case long-range repulsions between the bunched facets are negligible. But the relative weight of the secondary peaks in the TWD becomes significantly larger for those samples grown by H-assisted epitaxy. However, the data indicate that the extent of long-range repulsions does not increase with H dose but with the relative density of steps edges lying along directions different from the main one, i.e., $[1\bar{1}0]$. Specifically, the higher value of β corresponds to the sample exposed to H only during the surface cleaning step, which exhibits the higher $[1\bar{1}2]/[1\bar{1}0]$ step length ratio (Fig. 2(b)). Therefore, the new parameter β accounts for the extent of transverse meandering on the vicinal surface during near-equilibrium growth.

A second series of GaAs (110) samples (set B) with thicknesses between 100 and 500 ML were grown by conventional MBE at 430 °C to study the temporal evolution of the step-step interaction strength during kinetically driven step bunching. Figs. 3(a)–3(c) show $3\,\mu m \times 3\,\mu m$ AFM

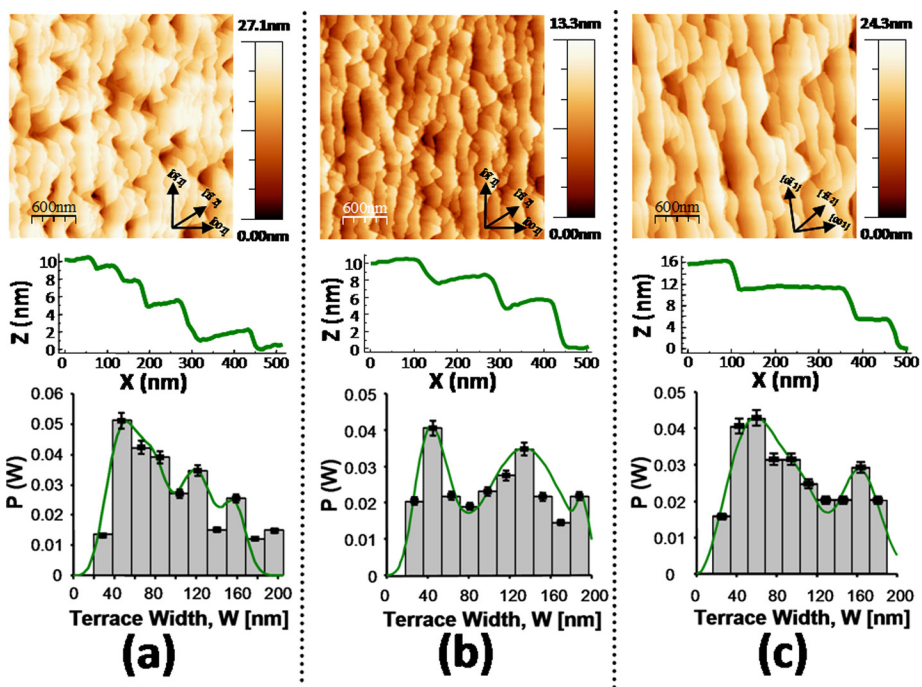

FIG. 3. AFM images ($3\,\mu m \times 3\,\mu m$) of the GaAs (110) surface morphology, typical cross-section profiles along the [001] tilt direction with the resulting terrace width histograms and fitted TWDs (solid line) after deposition of (a) 100 ML, (b) 200 ML, and (c) 600 ML GaAs at 430 °C with an As/Ga flux ratio of 30 in series B.

TABLE II. Fitting parameters used to simulate the experimental TWDs shown in Fig. 3 corresponding to **series B:** 100 ML, 200 ML, and 600 ML GaAs (110) grown by MBE at 430 °C with an As/Ga flux ratio of 30.

	Main peak							Secondary peaks				
Sample	γ (%)	W_{Wigner} (nm)	ρ	A_{Wigner}	α (%)	$W_{G\ short}$ (nm)	σ	β (%)	$W_{G\ large}$ (nm)	σ	S_H (nm)	W_0 (nm)
100 ML	29 ± 3	36 ± 5	3.5 ± 0.2	1.3 ± 0.4	100 ± 1			71 ± 6	$119 \pm 5/158 \pm 4$	$18 \pm 3/15 \pm 2$	5.3 ± 3.5	111 ± 0.3
200 ML	32 ± 3	44 ± 4	3.60 ± 0.05	1.44 ± 0.09	100 ± 1			68 ± 5	$134 \pm 2/191 \pm 3$	$30 \pm 1/14 \pm 1$	5.1 ± 2.2	125 ± 0.3
600 ML	59 ± 2	60 ± 2	1.90 ± 0.05	-0.05 ± 0.05	87 ± 4	108 ± 2	17 ± 1	41 ± 2	156 ± 9	20 ± 1	6.6 ± 4.0	160 ± 0.4

images of the surface morphology with the experimental terrace width histogram and the simulated TWDs (solid line) for 100 ML-, 200 ML-, and 600 ML-thick GaAs layers, respectively. All images show the formation of a multiatomic step morphology with terraces running along the main $[1\bar{1}0]$ direction. Previous dynamic reflective high energy electron diffraction (RHEED) studies in combination with AFM topography images have shown that, under the specified experimental conditions, bunching of $[1\bar{1}0]$ steps occurs from the onset of growth by preferential adatom incorporation from the upper terraces in the presence of *inverse* E-S step edge barriers.[10,30,32] The images in Figs. 3(a) and 3(b) also evidence that in the early stages of growth the surface is unstable against step meandering, exhibiting terraces laterally bounded by $[1\bar{1}n]$-type step edges ($n \geq 2$). Moreover, scanning electron microscopy studies have shown that these steps are constituted by staircases of monolayer and bilayer height steps and exhibit step edge rebonding through As-As dimer formation.[33] After 600 ML GaAs have been deposited, the formation of long terraces along $[1\bar{1}0]$, laterally bounded by the most stable step configuration $[1\bar{1}2]$, can be observed (Fig. 3(c)).

The TWDs in this series exhibit several damped oscillations, as predicted by KMC simulations of low temperature homoepitaxial growth in the presence of step edge barriers.[19] The simulation parameters used to fit the theoretical TWDs to the experimental histograms are shown in Table II, together with the average values of the terrace width and the bunched step height. The main peaks in the high step density region, which appear at 36 nm and at 44 nm for the 100 ML and the 200 ML GaAs samples, respectively, were accurately fitted to single Wigner functions ($\alpha = 100\%$). According to our simulations during the initial growth stages, the interactions between adjacent $[1\bar{1}n]$-type steps are moderately repulsive ($\rho = 3.5 - 3.6$) and they do not vary appreciably in strength up to 200 ML ($A_{Wigner} = 1.44$). After 600 ML GaAs deposition, the $[1\bar{1}0]$ bunched terraces have merged laterally and steps fluctuations are less pronounced. In this case, the skewed peak that appears in the high step density region of the TWD had to be fitted to a weighted sum of a Wigner and a Gaussian. The value of the parameter ρ extracted from the fit indicated that the effective step-step interaction at this growth stage was moderately attractive, i.e., $A_{Wigner} = -0.05$.

The observed changes in the interaction type and strength with GaAs thickness should be interpreted in terms of the kinetics-driven temporal evolution of the surface morphology as well as the characteristic topology and energetics of the step type that prevails as the step bunching instability approaches the steady state. In this sense, the present series clearly shows the existing differences in the interaction type between the two kinds of steps in the GaAs (110) vicinal surface, already anticipated by the results from series A. On the one hand, there exist strong energetic repulsions between adjacent $[1\bar{1}2]$-type steps, consistent with their tendency to form monolayer or bilayer height steps in this orientation, but not multiple-height step bunches. On the other hand, $[1\bar{1}0]$ steps have a higher energy than $[1\bar{1}2]$ ones[34] and bunching formation through attractive step-step interactions is energetically favoured, leading to the stabilization of the $[1\bar{1}0]$ step edge. Homoepitaxial growth on the GaAs (110) vicinal surface at low temperatures, i.e., 430 °C, is kinetically driven. Adatoms incorporate faster to $[1\bar{1}0]$ step edges, which form bunches from the onset of growth, and the surface topography is initially dominated by $[1\bar{1}n]$-type steps ($n \geq 2$), where growth is most likely controlled by the kinetics of As dimer breaking at the step edge prior to adatom incorporation. With further GaAs deposition, terraces grow and merge laterally in the $[1\bar{1}0]$ direction. As the steady state is approached, the rate of adatom incorporation to the $[1\bar{1}0]$ step edges slows down and the surface morphology is dominated by the $[1\bar{1}0]$ bunched terraces. The TWD on the surface during the initial growth stages thus samples primarily the energetic and entropic repulsions between wandering $[1\bar{1}n]$-type steps, whereas in the late stage regime the population of wandering $[1\bar{1}2]$ steps and hence the repulsive (energetic and entropic) interactions diminish and the TWD samples mainly the attractive step-step interactions in $[1\bar{1}0]$-oriented bunches.

Several Gaussians were necessary to fit the secondary peaks in the large-terrace region of the TWDs corresponding to the 100 ML and 200 ML GaAs samples. For these two samples, β is thus the sum of the specific weighs of the different Gaussian distributions. The large-terrace peak of the 600 ML-thick sample was in turn fitted to a single Gaussian. The large values of β obtained for the first two samples ($\beta \cong 70\%$) are consistent with the strong long-range repulsions generated by the large population of step bunches aligned along different $[1\bar{1}n]$ directions. As expected from the surface morphology evolution, the value of β diminishes in the late stage regime as the population of $[1\bar{1}0]$ bunched steps increases and the meandering instability tends to vanish, thus diminishing the long-range repulsive interactions between step bunches.

The third series of GaAs (110) samples (set C), having thicknesses between 25 and 500 ML, was deposited under

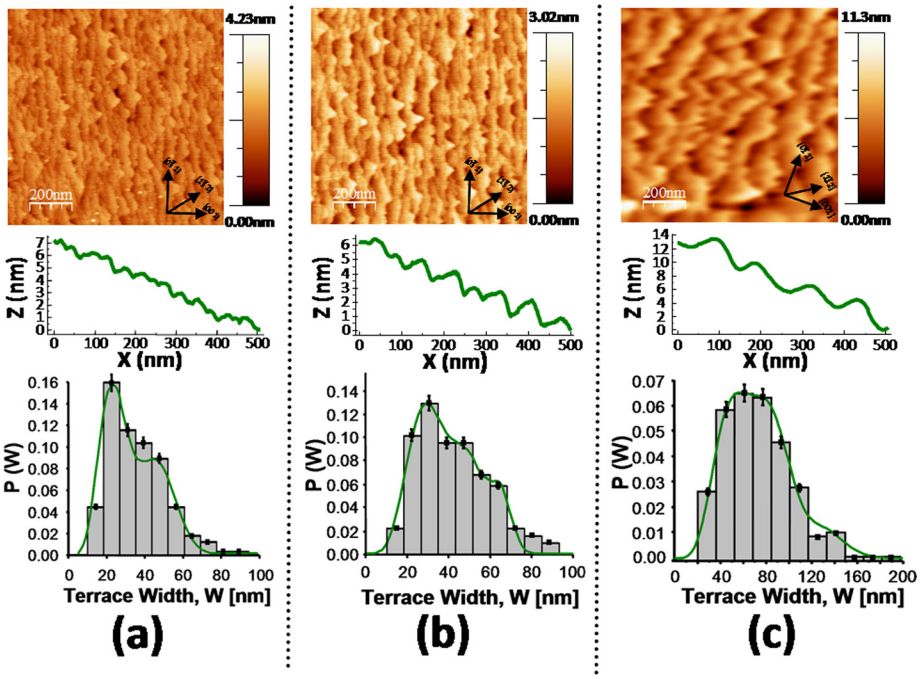

FIG. 4. AFM images ($1\,\mu m \times 1\,\mu m$) of the GaAs (110) surface morphology, typical cross-section profiles along the [001] tilt direction with the resulting terrace width histograms and fitted TWDs (solid line) after (a) 25 ML, (b) 50 ML, and (c) 500 ML GaAs deposition at 430 °C with an As/Ga flux ratio of 30 after H-assisted surface oxide cleaning in series C.

identical MBE conditions as set B (430 °C) following atomic H-assisted cleaning of the surface oxide. This series was grown to study the impact of chemisorbed H on the step-step interactions occurring during the development of kinetic step bunching. The AFM images ($1\,\mu m \times 1\,\mu m$) shown in Figs. 4(a)–4(c) depict the surface morphology after 25, 50, and 500 ML GaAs deposition. Underneath each image, we present the corresponding experimental terrace width histogram and the simulated TWD, fitted with the parameters shown in Table III. A strong tendency to form terraces bounded by meandering steps along $[1\bar{1}2]$ is observed at all growth stages examined. In contrast with those samples prepared by conventional MBE (set B), step bunching and step meandering coexist at all growth stages in this series. As shown in the table, the average values of the terrace width and multiatomic step height increase with layer thickness, but at a lower rate than in conventional MBE growth. Simultaneously, a progressive increase in the wavelength and self-organization of the meanders takes place.

For all three samples in set C, the main TWD peak in the high step density region was asymmetric and had to be fitted to a weighted sum of a Wigner and a Gaussian, while the shoulder in the large-terrace region was fitted to a single Gaussian. The results from fitting the main peaks located at 33 nm, 36 nm, and 68 nm for the 25 ML, 50 ML, and 500 ML thick GaAs (110) samples, respectively, revealed the existence of rather strong effective repulsions between adjacent steps, i.e., $\rho > 4$. The calculated values of A_{Wigner} decrease in the early growth stages, maintaining a constant value of 3.2 from 50 ML GaAs onwards. These results demonstrate that the steady state is reached at an earlier stage on the H terminated surface, thus corroborating the catalytic role of H in the GaAs (110) growth process observed by RHEED.[10] In addition, the stronger step-step interactions found for this series in comparison to the series of samples grown by conventional MBE at the same temperature (set B) stem not only from the increment of entropic repulsions originated by the narrower terraces, but, most importantly, from the energetic (dipole-induced) interactions between the H-terminated $[1\bar{1}2]$ steps. The latter becomes particularly relevant at low temperatures, where the exothermic reaction of H with the GaAs (110) surface leads to a higher H coverage of surface steps.[31]

The simulations also show that the main contribution to the TWD of the samples grown by H-MBE at low temperature comes from the secondary peak (shoulder) in the large-terrace region and its relative weight, measured by β, increases with layer thickness to a value of 85% after 500 ML GaAs deposition. This agrees with the progressive predominance of $[1\bar{1}2]$ versus $[1\bar{1}0]$-type steps and the strong long-range repulsions generated by the H-terminated $[1\bar{1}2]$ step bunches. It is worth noting the similar behaviour, in terms of β, shown by this

TABLE III. Fitting parameters used to simulate the experimental TWDs shown in Fig. 4 corresponding to series C: 25 ML, 50 ML, and 500 ML GaAs (110) grown by MBE at 430 °C with an As/Ga flux ratio of 30 after H-assisted oxide desorption.

	Main peak							Secondary peaks				
Sample	γ (%)	W_{Wigner} (nm)	ρ	A_{Wigner}	α (%)	$W_{G\ short}$ (nm)	σ	β (%)	$W_{G\ large}$ (nm)	σ	S_H (nm)	W_0 (nm)
25 ML	25 ± 8	33 ± 3	4.7 ± 0.2	3.2 ± 0.5	30 ± 5	45 ± 6	7 ± 1	75 ± 8	58 ± 3	5 ± 1	1.0 ± 0.3	42.0 ± 0.1
50 ML	18 ± 4	40 ± 10	4.3 ± 0.2	2.5 ± 0.5	43 ± 4	44 ± 8	6 ± 2	82 ± 8	60 ± 10	11 ± 3	1.3 ± 0.4	45.2 ± 0.1
500 ML	15 ± 1	68 ± 10	4.3 ± 0.4	2.5 ± 0.9	19 ± 7	85 ± 2	17 ± 1	85 ± 7	130 ± 10	18 ± 1	5 ± 1.0	76.1 ± 0.2

series and the first two samples in series B (100 ML and 200 ML), where bunching and extensive meandering of $[1\bar{1}2]$ steps coexist. Therefore, the data show that the new parameter β is a reliable indicator of the extent of transverse meandering also for low temperature growth.

V. CONCLUSION

The step-step interactions in facets, step bunches, and step meanders have been investigated for various homoepitaxial GaAs (110) surface patterns through the quantitative analysis of the terrace width distribution. A good agreement was found between the experimental TWDs determined from AFM measurements and those derived from numerical calculations based on a combination of Gaussian and Wigner distributions. In all cases, the TWD exhibits a main peak in the high step density (short-terraces) region and one or two secondary peaks in the low step density (large terraces) region. High temperature faceting results from attractive interactions between straight $[1\bar{1}0]$ steps and the TWD is composed almost exclusively by the short-terrace peak. Kinetic step bunching at low temperatures initially coexists with transverse meandering, resulting in a TWD that samples mainly the entropic and energetic repulsions between the $[1\bar{1}n]$-oriented meandering steps. But in the steady state regime, meandering is highly reduced due to lateral merging of terraces and the attractive interactions between the $[1\bar{1}0]$ bunched steps become dominant, leading to a TWD with a higher relative weight of the short-terrace peak. Chemisorbed H reduces the strength of attractive interactions between $[1\bar{1}0]$ bunched steps and modifies the distribution of terrace widths, particularly at low temperatures where the H coverage on the GaAs (110) surface is larger. Under such conditions, the TWD is consistent with the presence of entropic and dipole-induced energetic repulsions between H-terminated $[1\bar{1}2]$ meandering steps. Finally, a direct correlation has been found between the value of the adjustable parameter β, which accounts for the relative weight of the secondary peaks of the TWD in our model, and the extent of transverse meandering on the vicinal surface.

ACKNOWLEDGMENTS

This work was funded by MICINN (Spain) under Grants TEC2007-66955 and MAT2011-22536, and by the EU-FP7 MAT ERA-Net "ENGAGE" project, with local support provided by Fundación Madri+d. M.B. gratefully acknowledges Intel Ireland Academic Council for a postgraduate scholarship. B.G acknowledges a Juan de la Cierva post-doctoral contract from MICINN.

[1]Y. M. Yu and B.-G. Liu, Phys. Rev. B **73**, 035416 (2006).
[2]P. Tejedor, L. Díez-Merino, I. Beinik, and C. Teichert, Appl. Phys. Lett. **95**, 123103 (2009).
[3]L. Díez-Merino and P. Tejedor, J. Appl. Phys. **110**, 013106 (2011).
[4]G. Ehrlich and F. G. Hudda, J. Chem. Phys. **44**, 1039 (1966).
[5]R. L. Schwoebel, J. Appl. Phys. **40**, 614 (1969).
[6]G. S. Bales and A. Zangwill, Phys. Rev. B **41**, 5500 (1990).
[7]J. Kallunki and J. Krug, Phys. Rev. B **65**, 205411 (2002).
[8]J. Myslivecek, C. Schelling, F. Schäffler, G. Springholtz, P. Smilauer, J. Krug, and B. Voigtländer, Surf. Sci. **520**, 193 (2002).
[9]M. Vladimirova, A. De Vita, and A. Pimpinelli, Phys. Rev. B. **64**, 245420 (2001).
[10]P. Tejedor, M. L. Crespillo, and B. A. Joyce, Mater. Sci. Eng., C **26**, 852 (2006).
[11]E. E. Gruber and W. W. Mullins, J. Phys. Chem. Solids **28**, 875 (1967).
[12]N. C. Bartelt, T. L. Einstein, and E. D. Williams, Surf. Sci. **240**, L591 (1990).
[13]T. L. Einstein and O. Pierre-Louis, Surf. Sci. Lett. **424**, L299 (1999).
[14]O. Pierre-Louis and C. Misbah, Phys. Rev. B **58**, 2259 (1998).
[15]E. L. Goff, L. Barbier, L. Masson, and B. Salanon, Surf. Sci. **432**, 139 (1999).
[16]M. L. Metha, *Random Matrices*, 3rd ed. (Academic, New York, 2004).
[17]F. Calogero, J. Math. Phys. **10**, 2191 (1969).
[18]B. Sutherland, J. Math. Phys. **12**, 246 (1971).
[19]A. Videcoq, A. Pimpinelli, and M. Vladimirova, Appl. Surf. Sci. **177**, 213 (2001).
[20]A. Pimpinelli, H. Gebremariam, and T. L. Einstein, Phys. Rev. Lett. **95**, 246101 (2005).
[21]T. L. Einstein, Appl. Phys. A **87**, 375 (2007).
[22]M. Lässig, Phys. Rev. Lett. **77**, 526 (1996).
[23]M. Giesen and T. L. Einstein, Surf. Sci. **449**, 191 (2000).
[24]H. L. Richards, S. D. Cohen. T. L. Einstein, and M. Giesen, Surf. Sci. **453**, 59 (2000).
[25]S. D. Cohen, R. D. Schroll, T. L. Einstein, J.-J. Métois, H. Gebremariam, H. L. Richards, and E. D. Williams, Phys. Rev. B **66**, 115310 (2002).
[26]T. L. Einstein, H. L. Richards, S. D. Cohen, and O. Pierre-Louis, Surf. Sci. **493**, 460 (2001).
[27]W. W. Pai, J. S. Ozcomert, N. C. Bartelt, and T. L. Einstein, Surf. Sci. **307–309**, 747 (1994).
[28]V. B. Shenoy, S. Zhang, and W. F. Saam, Phys. Rev. Lett. **81**, 3475 (1998); Surf. Sci. **467**, 58 (2000).
[29]C. Odin, J. P. Aimé, Z. El Kaakour, and T. Bouhacina, Surf. Sci. **317**, 321 (1994).
[30]P. Tejedor, M. L. Crespillo, and B. A. Joyce, Appl. Phys. Lett. **88**, 063101 (2006).
[31]S. Nannarone and M. Pedio, Surf. Sci. Rep. **51**, 1 (2003).
[32]P. Tejedor, F. E. Allegretti, P. Šmilauer, and B. A. Joyce, Surf. Sci. **407**, 82 (1998).
[33]Y.-N. Yang, B. M. Trafas, R. L. Siefert, and J. H. Weaver, Phys. Rev. B **44**, 3218 (1991).
[34]J. M. McCoy and J. P. LaFemina, Phys. Rev. B **54**, 14511 (1996).